Improvement of an Electromagnetic-Thermal-Mechanical Coupled Simulation for the Optimization of Complex Processes in Induction Hardening

Benjamin Dollhofer[1,*1], Stefan Dietrich[1] and Volker Schulze[1]

[1]*Institute for Applied Materials – Materials Science and Engineering (IAM-WK) / Karlsruhe Institute of Technology (KIT), 76131 Karlsruhe, Germany*

Induction surface hardening is mainly used in industrial applications to increase the lifetime of components with high efficiency. Improving the predictability of the process is essential for their further development. The current study presents an analysis of a finite element method for an indirect coupled electromagnetic thermal-mechanical simulation to investigate the inductive heating during surface hardening. In particular, the sensitivity of the coupling of electromagnetic and thermal-mechanical simulation was analyzed. An optimized time step was introduced, which reduces the simulation time without affecting the accuracy. More importantly, the study shows, that a high time step only leads to minor deviations in the resulting temperature profile, which simplifies the simulation of longer and more complex heat treatment strategies, especially for processes below the Curie temperature.

Keywords: *induction heating, surface hardening, finite element method, electromagnetics, optimized time step*

1. Introduction

Induction surface hardening is an established and resource-saving process for the heat treatment of steel components. One particular problem is its difficulty of prediction, especially in the case of ferromagnetic materials. Reasons are the strong dependence of the magnetic properties of the workpiece on temperature and its non-linear behavior, notably with longer process times and in temperature ranges close and above the Curie temperature [1,2)]. An accurate prediction of the mechanisms occurring in the heating process is becoming increasingly relevant with regard to the development of further potential in the field of inductive surface hardening, like the investigation on bainitic-martensitic mixed microstructure with the objective of increasing the component durability [3,4)].

For most of the existing simulation models, there is a choice between accuracy and computational cost. Also, they may be limited by the capabilities of the simulation environment, including temperature dependent material properties and phase transformations. The focus is often on reducing or simplifying the proportion of electromagnetic simulation, as it is in general the most time-consuming part of the simulation. Several studies investigated simplifications and optimal adaptations of the magnetization curves of ferromagnetic materials to improve the electromagnetic model [5–7)]. Often indirectly or weakly coupled simulation models are used, which solves the electromagnetic and the thermal-mechanical model separately and then combines the results in an iterative way. Previous studies have shown that the complexity of the electromagnetic model can be reduced by including analytical models [8,9)]. Furthermore, so called multi-fidelity optimization approaches can support the electromagnetic and the thermal-mechanical model as well [10)]. In fact, these investigations already have led to excellent simulation results of the material properties with a large reduction of the process time for AISI 4140.

This work focusses on another aspect, namely the possibility of using electromagnetic simulation as efficiently as possible without introducing additional models. For this purpose, the simplification using a fictive permeability for ferromagnetic materials proposed by D. Labridis et al. [7)] has been studied, introducing an optimized coupling between the electromagnetic and thermal-mechanical systems. Finally, an induction surface hardening process was simulated with AISI 4140, including a heating and a quenching step.

2. Methods

2.1 Simulation framework

The current simulation and material model is based on the previous works of M. Schwenk [11)] and D. Kaiser et al. [12,13)]. As seen in Figure 1, an indirectly coupled, also called weakly coupled, electromagnetic-thermal finite element method is applied [1)]. The simulation framework is Abaqus 2019 using custom subroutines. The control as well as the data transfer between the individual sections of the simulation are programmed in Python.

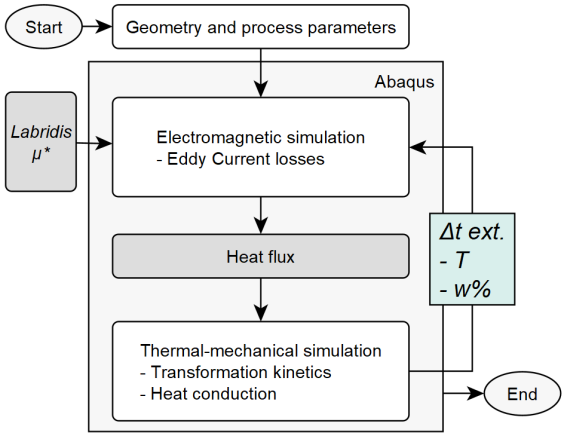

Figure 1:Schematic representation of the simulation framework

2.1.1 Electromagnetic Simulation

The model first solves the electromagnetic simulation to estimate the eddy current losses. D. Labridis et al. introduced a linear magnetization curve that is congruent to the

*1 Phd student, KIT

hysteresis of the magnetization curve of ferromagnetic materials and thus, makes it possible to calculate the electromagnetic simulation with a time harmonic approach[7]. This leads to a much more efficient steady-state simulation compared to a step-by-step simulation of the eddy current losses. The electromagnetic simulation is executed iteratively via a Python script. Thereby, the resulting fictive permeability in the workpiece μ^* is calculated for each element until the changes in the simulation result are within a specified tolerance. Phase fractions with ferromagnetic properties like ferrite, bainite or martensite and austenitic fractions with paramagnetic properties are considered, but constant for each element during the simulation step. After that, the generated Joule heat is passed to the transient thermal-mechanical simulation as a body heat flux using it as a boundary condition for the thermal-mechanical step.

2.1.2 Thermal-mechanical Simulation

The structure of the thermal-mechanical material model used in the simulation has been described and discussed in previous publications [12–15]. In this step, the phase transformation as well as the mechanical properties are determined. The resulting phase fractions w_i as well as the resulting temperature profile of the heat conduction inside the part are transferred to the next step of the electromagnetic simulation. The iteration step that connects both models of the simulation is also called external iteration step or external time step Δt_{ext}, and is determined by the duration of the transient thermal-mechanical simulation.

2.2 Model geometry

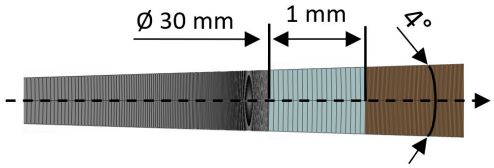

Figure 2: Schematic representation of the model geometry in Abaqus 2019

As shown in Figure 2, The geometry of the simulated specimen corresponds to a shaft with a diameter of 30 mm, whereby only a circular section of 4° with an axial length of 0.01 mm was simulated in order to reduce the computational cost. The distance to the inductor is 1 mm radial. A bias along the radial axis, with a minimum of 0.002 mm and a maximum of 0.2 mm was used for the workpiece. While the electromagnetic model accounts for workpiece, inductor, field concentrator and surrounding air, the thermal-mechanical model was reduced to the workpiece. This leads to a thermal-mechanical model, which consists of a total of 556 elements, and an electromagnetic model, which contains a total of 1128 elements. The boundary conditions were chosen to exploit the symmetry of the assembly.

2.3 Implementation of the optimized external time step

The external time step Δt_{ext} is the core of this investigation and the only parameter that was changed during this study. The assumption is that the permeability and its temporal course are decisive for the course of the eddy currents losses in the process and thus, for the heat flow in the workpiece. The hysteresis of the magnetization curve and therefore the fictive permeability for AISI 4140 changes only slightly up to a temperature of 673 K and starts to drop drastically after a temperature of 873 K, until it approaches the magnetic field constant at the Curie temperature [11]. The Curie temperature for this simulation is set to 1026 K.

To determine Δt_{ext} a simulation is performed with a relatively large time step of 0.2 s to get a first temperature profile. Analyzing this profile and its temperature gradient compared to the initial condition of the workpiece, a time step is calculated using the current maximum heating rate, the current maximum temperature and the target temperature of 873 K. For the next time step, the previous temperature profile is used in the same way until the target temperature is reached or exceeded. After exceeding this temperature, a minimum time step of 0.01 s was set, which is maintained until the end of the heating process.

3. Results

In Figure 3 (a) the temperature curve as well as the curve of the fictive permeability μ^* of an element over time at the edge of the workpiece is visualized. The inductor frequency is set to 30 kHz and a heating rate of ~1015 K/s is chosen. The curves show the development at different external time steps Δt_{ext}. The optimized time step and the time step with an increment of 0.1 s were additionally illustrated with vertical lines in the corresponding color to visualize the effect on the respective temperature curves. In Figure 3 (b) the development of the austenite fraction w_a during the phase transformation is visualized.

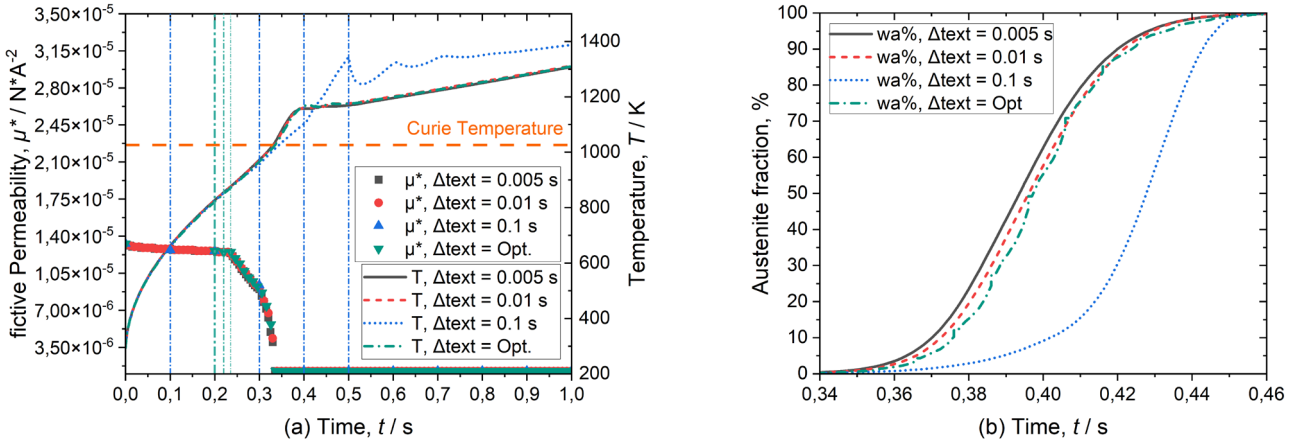

Figure 3: (a) Profile of temperature and fictive permeability during induction heating; (b) Profile of the austenite fractions during phase transformation

The simulation time t and maximum temperature T_{max} after 1 s induction heating are listed in Table 1. Furthermore, the maximum hardness HV_{max} at the edge after quenching and the surface hardening depth *Shd* were compared. The surface hardening depth is defined as the distance from the surface with a decrease in hardness to 575 HV [16]. Since the total simulation time strongly depends on the processor power and the number of CPUs used, only the relative values of the total simulation time are shown. The simulation time for the highest resolution of Δt_{ext}. was 49 hours. Further simulations with different frequencies and heating rates showed similar results and tendencies.

Table 1: Values for the simulation with ~1015 K/s heating rate

Δt_{ext}	t %	T_{max}	HV_{max}	*Shd*
0.1 s	4%	1387 K	729,09 HV	2,08 mm
0.01 s	47%	1314 K	729,16 HV	2,01 mm
0.005 s	100%	1308 K	729,16 HV	2,00 mm
Opt.	16%	1310 K	729,11 HV	1,99 mm

4. Discussion

A similar profile of the austenite fraction w_a and fictive permeability μ^* is accompanied by the same temperature history. This is significant for a constant but too large time step, which leads to a poor temporal grid when the Curie temperature is exceeded and changing phase fractions were underestimated. As a consequence, an inappropriate heat flow is calculated during the electromagnetic simulation. Below the Curie temperature, the changes in the magnetic properties due to a rising temperature is mainly responsible for changes within the temperature curves. Above the Curie temperature, this change is extensively accelerated by the starting austenite formation. At 0.4 s, the maximum austenite fraction at the boundary is ~62% for Δt_{ext} with higher resolutions and only 9% for Δt_{ext} with 0.1 s. Thus, the eddy current losses and therefore the heat flow of the large resolution step is overestimated, making a difference in austenite fraction the main cause of the differences in the temperature field.

As the simulation progresses, the austinite fraction equalizes, which in turn leads to a similar heating rate and an alignment of the temperature curves. At the end of the heating cycle, the maximum temperature with a Δt_{ext} of 0.1 s is higher than the maximum temperature of the simulations with a higher Δt_{ext} resolution. The difference in the temperature profile results also in a slightly higher hardening depth. The optimized time step comes to an accurate result with a reduction in simulation time of 65% compared to the simulation with a constant Δt_{ext} of 0.01 s. Doing the same comparison for the simulation with a constant Δt_{ext} of 0.1 s, it still comes to an acceptable result while reducing the simulation time to 91%.

In summary, the massive reduction in simulation time with a relatively large time step allows qualitatively sufficient statements about the hardening process. This is especially valid if the maximum workpiece temperature during the process remains below the Curie temperature and without starting the austenite phase transformation.

5. Conclusions

The analysis of the external time step revealed significant differences especially for process routes with a heating above the Curie temperature, particularly if the time grid only poorly fits the crossing of this temperature as well as the start of the austenite formation. By optimizing the time step, the process time could be reduced up to 65% while maintaining a high accuracy. However, the use of a rough external time step of 0.1 s is still a good compromise in terms of reducing simulation time about 91%.

Consequently, the use of large external time steps in the simulation of processes such as inductive tempering or inductive austempering of AISI 4140, should lead to accurate results in investigating component behavior, especially when the maximum temperature remains below the Curie temperature.

References

1) V. Rudnev, D. Loveless, and R. L. Cook, eds., *Handbook of Induction Heating* (CRC Press, 2017).

2) V. Rudnev, Heat treating progress (2004) pp. 23–25.

3) F. Mühl, J. Jarms, D. Kaiser, S. Dietrich, and V. Schulze, Materials & Design **195** (2020) pp. 108964.

4) c. H. Young and H. K. D. H. Bhadeshia, Materials Science and Technology **10** (1994) pp. 209–214.

5) M. Baldan, M.-H. Stolte, B. Nacke, and F. Nurnberger, IEEE Trans. Magn. **56** (2020) pp. 1–9.

6) M. Fisk, M. Ristinmaa, A. Hultkrantz, and L.-E. Lindgren, Applied Mathematical Modelling **111** (2022) pp. 818–835.

7) D. Labridis and P. Dokopoulos, IEEE Trans. Magn. **25** (1989) pp. 2665–2669.

8) M. Areitioaurtena, U. Segurajauregi, V. Akujärvi, M. Fisk, I. Urresti, and E. Ukar, Adv. Model. and Simul. in Eng. Sci. **8** (2021).

9) M. Areitioaurtena, U. Segurajauregi, I. Urresti, M. Fisk, and E. Ukar, Procedia CIRP **87** (2020) pp. 545–550.

10) M. Baldan, A. Nikanorov, and B. Nacke, COMPEL **39** (2019) pp. 133–143.

11) M. Schwenk (2012) [DOI: 10.5445/KSP/1000030463] [in de].

12) D. Kaiser (2019) [DOI: 10.5445/IR/1000100278] [in de].

13) D. Kaiser, J. Damon, F. Mühl, B. de Graaff, D. Kiefer, S. Dietrich, and V. Schulze, Journal of Materials Processing Technology **279** (2020) pp. 116485.

14) P. Schüßler, J. Damon, F. Mühl, S. Dietrich, and V. Schulze, Computational Materials Science **221** (2023) pp. 112079.

15) F. Mühl, J. Damon, S. Dietrich, and V. Schulze, Computational Materials Science **184** (2020) pp. 109916.

16) *DIN EN ISO 18203:2022-07, Stahl_- Bestimmung der Dicke gehärteter Randschichten (ISO_18203:2016); Deutsche Fassung EN_ISO_18203:2022* (Beuth Verlag GmbH, Berlin).